Traffic

doi:10.1111/tra.12269

Microtubule Motors Power Plasma Membrane Tubulation in Clathrin-Independent Endocytosis

Charles A. Day[1,2], Nicholas W. Baetz[1], Courtney A. Copeland[1], Lewis J. Kraft[3], Bing Han[1], Ajit Tiwari[1], Kimberly R. Drake[1], Heidi De Luca[4], Daniel J.-F. Chinnapen[4], Michael W. Davidson[5], Randall K. Holmes[6], Michael G. Jobling[6], Trina A. Schroer[7], Wayne I. Lencer[4,8] and Anne K. Kenworthy[1,3,9,10]*

[1]Department of Molecular Physiology and Biophysics, Vanderbilt University School of Medicine, Nashville, TN, USA
[2]Current address: Hormel Institute, University of Minnesota, Austin, MN, USA
[3]Chemical and Physical Biology Program, Vanderbilt University, Nashville, TN, USA
[4]GI Cell Biology, Department of Pediatrics, Boston Children's Hospital, Boston, MA, USA
[5]National High Magnetic Field Laboratory, The Florida State University, Tallahassee, FL, USA
[6]Department of Immunology and Microbiology, University of Colorado School of Medicine, Aurora, CO, USA
[7]Department of Biology, The Johns Hopkins University, Baltimore, MD, USA
[8]Harvard Medical School and the Harvard Digestive Diseases Center, Boston, MA, USA
[9]Department of Cell and Developmental Biology, Vanderbilt University School of Medicine, Nashville, TN, USA
[10]Epithelial Biology Program, Vanderbilt University School of Medicine, Nashville, TN, USA
*Corresponding author: Anne K. Kenworthy, Anne.kenworthy@vanderbilt.edu

Abstract

How the plasma membrane is bent to accommodate clathrin-independent endocytosis remains uncertain. Recent studies suggest Shiga and cholera toxin induce membrane curvature required for their uptake into clathrin-independent carriers by binding and cross-linking multiple copies of their glycosphingolipid receptors on the plasma membrane. But it remains unclear if toxin-induced sphingolipid crosslinking provides sufficient mechanical force for deforming the plasma membrane, or if host cell factors also contribute to this process. To test this, we imaged the uptake of cholera toxin B-subunit into surface-derived tubular invaginations. We found that cholera toxin mutants that bind to only one glycosphingolipid receptor accumulated in tubules, and that toxin binding was entirely dispensable for membrane tubulations to form. Unexpectedly, the driving force for tubule extension was supplied by the combination of microtubules, dynein and dynactin, thus defining a novel mechanism for generating membrane curvature during clathrin-independent endocytosis.

Keywords cholera toxin, clathrin-independent endocytosis, dynactin, dynein, membrane curvature, microtubules

Received 30 January 2015, revised and accepted for publication 6 February 2015, uncorrected manuscript published online 18 February 2015, published online 27 April 2015

Endocytosis, the process of internalizing vesicles or tubules and their associated cargo from the cell surface, serves essential functions for all cell types. Two general mechanisms of membrane uptake have been described. One involves the assembly of a rigid clathrin coat on the cytoplasmic surface of the plasma membrane that generates a highly curved membrane invagination, sequesters cargo and facilitates membrane fission and budding from the cell surface for trafficking into the cell (1). The other mechanism is clathrin-independent, and consists of multiple pathways, but how clathrin-independent carriers are generated remains poorly understood (2–9).

The AB_5 subunit toxins cholera (CTx) and Shiga toxin (STx) have become widely used as model cargoes for studying clathrin-independent endocytosis, including uptake via tubular endocytic carriers (10–25). Both toxins bind plasma membrane glycosphingolipids, and contain five or fifteen receptor binding sites for high-avidity association with cells via their respective B-subunits (26,27). Receptor

cross-linking is dispensable for CTx intoxication of host cells (28,29), but it is clear that CTx and STx binding to multiple glycosphingolipid receptors affects the membrane dynamics of uptake and intracellular trafficking in ways that enhance their toxicity (18,30). One way this is thought to occur is via a novel clathrin-independent mechanism in which toxin binding induces negative curvature of the plasma membrane (18,31). This mechanism has been best described for the B-subunit of Shiga toxin (STxB), but is also utilized by the B-subunit of cholera toxin (CTxB) and the glycosphingolipid-binding virus simian virus 40 (18,30).

According to this model, toxin binding deforms the membrane beneath the toxin by compacting the glycosphingolipids and/or by reorienting them to form a curved surface (18,30). In support of this idea, STxB or CTxB binding to giant unilamellar lipid vesicles (GUVs) causes inwardly directed tubulations of these artificial lipid membranes. Similarly, in live cells subjected to treatments that block membrane scission, toxins accumulate in tubular invaginations originating from the plasma membrane, analogous to those seen in GUVs (18,30). These microns-long structures are devoid of markers of clathrin-dependent endocytosis and can form even under conditions where cellular ATP is depleted (18). Toxin-induced changes in membrane organization are thought to be important for their formation, operating from outside the cell to form plasma membrane tubules in the absence of active cellular processes. But it remains unclear how toxin binding could supply the mechanical force needed to form the microns-long membrane invaginations observed in cells under these conditions. To what extent host cell factors contribute to this process is also uncertain, as few endogenous cellular regulators of this pathway have been identified. To address these questions, we investigated the mechanisms responsible for plasma membrane deformation during clathrin-independent endocytosis of CTxB in live cells.

Results

Assay for analysis of tubulation of the plasma membrane

To study mechanisms that participate in bending the plasma membrane during clathrin-independent endocytosis, we took advantage of a previously described assay that traps STxB and CTxB in surface attached tubules thought to correspond to stalled endocytic intermediates (18,30). Several conditions facilitate the growth of surface attached tubular invaginations containing fluorescently labeled toxins, including ATP depletion, actin disruption, cholesterol depletion and inhibition of dynamin. These conditions are thought to be permissive for tubule growth, but prevent tubule scission, leading to the accumulation of toxin within these structures.

CTxB accumulated in linear, microns-long tubules in ATP-depleted cells and/or when actin was either disrupted or stabilized (Figures 1A–D and S1). Control experiments revealed that STxB and CTxB localized to the same tubules in cells incubated with both toxins, supporting the idea they are formed by a common mechanism (Figure S1D). We also found that the tubules were rapidly labeled by a second application of CTxB after they had formed, confirming that the tubules originated from the plasma membrane and were surface attached for the time course of these studies (Figure S1E). In cells treated with the dynamin inhibitor Dynasore, irregular branched networks of tubules were observed (Figure 1E), resembling those seen before in cells expressing a Dynamin1 K44A mutant (17). These findings confirm that CTxB readily associates with membrane tubules under a variety of conditions that inhibit scission, thus allowing us to further study requirements for tubule formation.

Binding to a single GM1 is sufficient to support the association of cholera toxin with tubular invaginations

Current models propose compaction of glycosphingolipids by toxin binding plays an essential role in initiating membrane curvature and tubulating the membrane to form plasma membrane invaginations (18). A mutant form of STxB lacking the Gb_3 binding site III demonstrated greatly reduced ability to drive tubule formation in cells, suggesting multiple glycosphingolipid binding sites enhance the ability of toxins to deform membranes (18). To test if cholera toxin binding causes plasma membrane tubulations by compacting or reorienting multiple glycosphingolipids into a curved surface in a similar manner, we first studied a mixture of chimeric cholera toxins ($CTx_{chimera}$) that bind 0, 1 or 2 glycosphingolipid

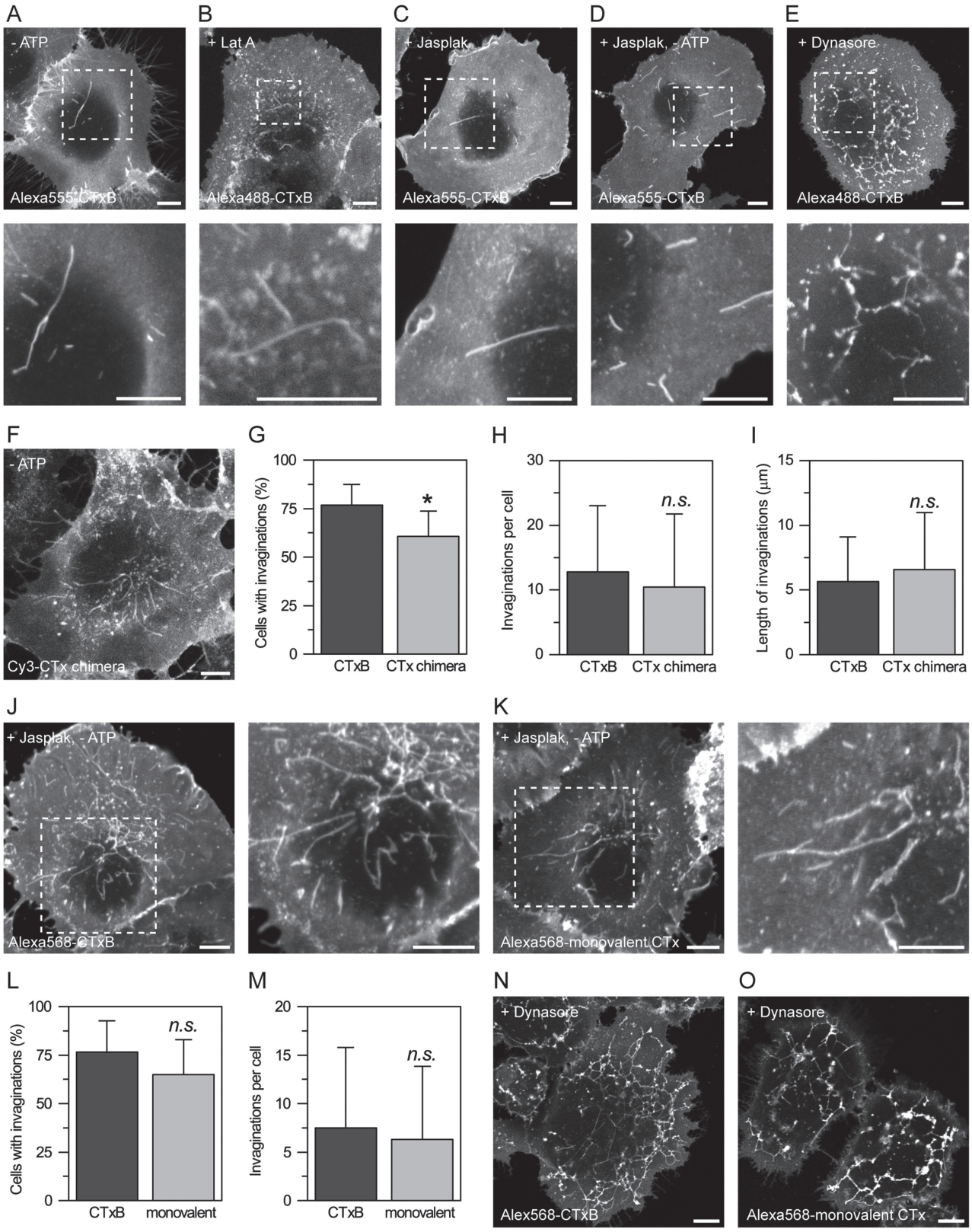

Figure 1: Legend on next page.

receptors (ganglioside GM_1) instead of the usual 5 (28). Unexpectedly, the chimeric mutant toxins were readily observed in tubular invaginations in ATP-depleted cells, and the average number of invaginations per cell and length of the invaginations were similar for wild type and chimeric toxins (Figure 1F–I). We next asked if a toxin with only a single GM_1 binding site (monovalent CTx) (29) can be directed to tubules. Strikingly, this monovalent CTx was localized within tubular invaginations as well (Figure 1J–O), suggesting that toxin-induced crosslinking of GM_1 is dispensable for tubule formation.

Toxin binding is dispensable for tubule formation

The finding that extensive crosslinking of GM_1 is not required for tubules to form suggests that the elongated tubules containing CTx may be generated by machinery endogenous to the host cell. If so, cellular plasma membrane proteins should also be found in the tubular invaginations in the absence of bound toxin. To test this, we first screened several cell surface markers for co-localization with CTxB in tubular invaginations. Several cell surface proteins were found to extensively label tubular structures even in the absence of CTxB binding (Figures 2 and S2). As one example, the cytosolic plasma membrane-associated protein HRas (GFP-HRas) strongly localized to the tubular invaginations both in the presence of CTxB and independently of CTxB in response to ATP-depletion, actin disruption or actin stabilization (Figure 2A–F). In ATP-depleted cells, a similar number of GFP-HRas positive tubules were found in the presence (18 ± 15, $n = 26$ cells) or absence (18 ± 11, $n = 23$ cells) of CTxB, suggesting they form by the same mechanism. Tubule formation was not stimulated by the GTPase activity of Ras, because a minimal membrane targeted form of GFP, GFP-HRas tail, also labeled tubules (Figure 2G,H). Thus, tubulation of the plasma membrane can occur in the absence of toxin-induced cross-linking of glycolipids, indicating that the driving force(s) for tubule extension can be generated by factors endogenous to the host.

An intact microtubule network is required for the formation of extended tubular invaginations

It is well known that microtubules and microtubule motors are capable of deforming membranes (32–34). Such mechanisms are not currently thought to contribute to the early stages of endocytosis (32). However, CTxB has previously been found to localize within microtubule-dependent tubular invaginations of intact BSC1 cells, suggesting a microtubule-dependent process of toxin uptake (13). Consistent with these findings, we noticed that the tubular invaginations containing CTxB in ATP-depleted cells were often directed toward the cell center in an orientation typifying the microtubule network (Figures 1F,J and 2A) and that the microtubule networks remained intact after ATP depletion (Figure 3A). Tubular invaginations containing CTxB were also often found aligned closely with taxol-stabilized microtubules (Figure 3B,C).

When imaged over time (Movies S1 and S2), the tubules sometimes grew smoothly (Figure 3D–F), but were often observed to pause and undergo bi-directional motions (Figure 3G–I) and branching events (Figure 3J) characteristic of microtubule-dependent motions. We thus asked if the microtubule network was required for tubular invaginations to form. Remarkably, disruption of microtubules prior to CTxB binding led to a complete loss of tubular

Figure 1: No more than one functional GM_1 binding site is required to target cholera toxin to plasma membrane invaginations. A–E) CTxB accumulates in either linear extended tubules (A–D) or branched tubules (E) under conditions that block scission. Bar, 10 μm. (F–M) Cholera toxin binding mutants accumulate in tubular invaginations. F) Cy3-CTx chimera labels tubules in ATP depleted COS-7 cells. G–I) Quantification of invaginations in ATP-depleted cells labeled with Cy3-CTx chimera or Alexa555-CTxB. G) Percentage of cells displaying invaginations (mean ± SD from 117–119 cells). *, $p < 0.05$, chi-squared test. H) Average number of invaginations per cell (mean ± SD of 42–46 cells). *n.s.*, $p > 0.05$; Student *t*-test. I) Length of invaginations (mean ± SD for 219–332 invaginations). *n.s.*, $p > 0.05$; Student *t*-test. J–M) Both wild type CTxB and monovalent CTx accumulate in tubular invaginations in cells subjected to Jasplakinolide pretreatment prior to ATP depletion. L) Percentage of cells displaying invaginations. (mean ± SD of 59–63 cells). *n.s.*, $p > 0.05$; chi-squared test. M) Average number of invaginations per cell. (mean ± SD of 59–63 cells). *n.s.*, $p > 0.05$; Student *t*-test. N and O) Similar to wild type CTxB, monovalent CTx accumulates in branched tubules in Dynasore-treated cells. Bars, 10 μm.

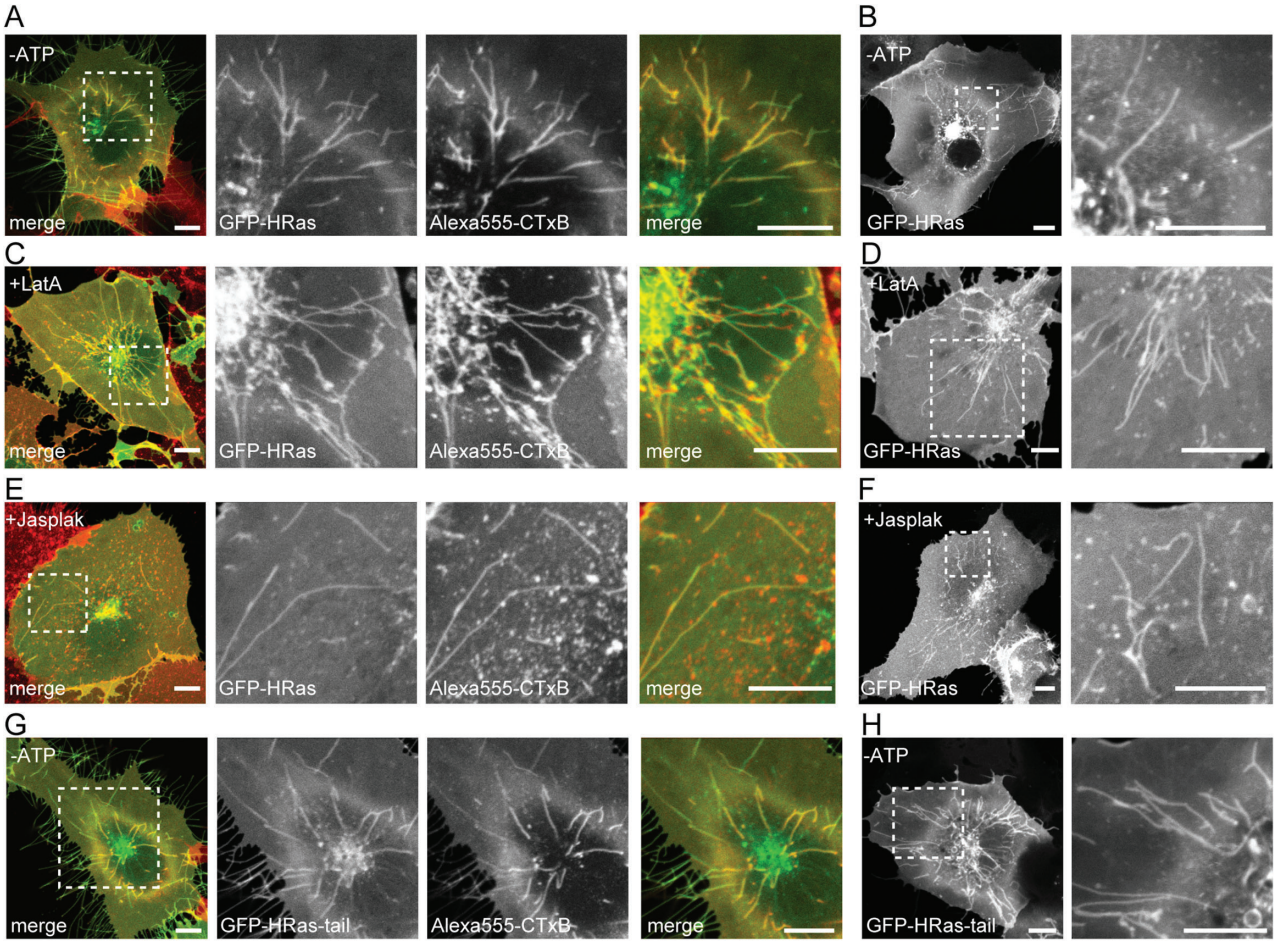

Figure 2: Toxin binding is not necessary for tubular invaginations to form. A,B) EGFP-HRas (green) is found in plasma membrane invaginations in ATP-depleted cells in both the presence (A) and absence (B) of Alexa555-CTxB (red). C–F) Similar results were obtained for GFP-HRas in cells subjected to actin disruption (C and D) or actin stabilization (E and F). G and H) A construct containing only the C-terminal 10 amino acids of HRas, EGFP-HRas-tail (green), also localized to tubules in both the presence and absence of CTxB. Bars, 10 μm.

invaginations containing the toxin in ATP-depleted cells (Figure 4A,C). Microtubule disruption also inhibited the formation of tubules containing CTxB or monovalent CTx in cells subjected to dynamin inhibition, actin disruption or actin stabilization (Figure 4E,F; Figure S3A,B). Thus, the extended tubular invaginations are strongly microtubule dependent.

Microtubule plus end dynamics are not required for the growth of tubular invaginations

To elucidate how microtubules might support tubulation of the plasma membrane, we first considered a mechanism in which interactions between membranes and dynamic microtubules are mediated by plus-end binding proteins to drive endomembrane translocation (35–39). To test this possibility, we monitored the plus-end binding protein GFP-EB3 (40). In ATP-depleted cells, GFP-EB3 still labeled microtubules, but was no longer concentrated at their tips (Movie S3), indicating enrichment of plus-end binding proteins at microtubule ends cannot be required for tubule formation. Furthermore, pretreating cells with low doses of nocodazole (150 nM) to suppress microtubule plus-end dynamics (40–42) had no detectable effect on the number of ATP-depleted cells that contained CTxB-positive invaginations (Figure 4B,D). Dynamic microtubule growth thus cannot explain tubule extension.

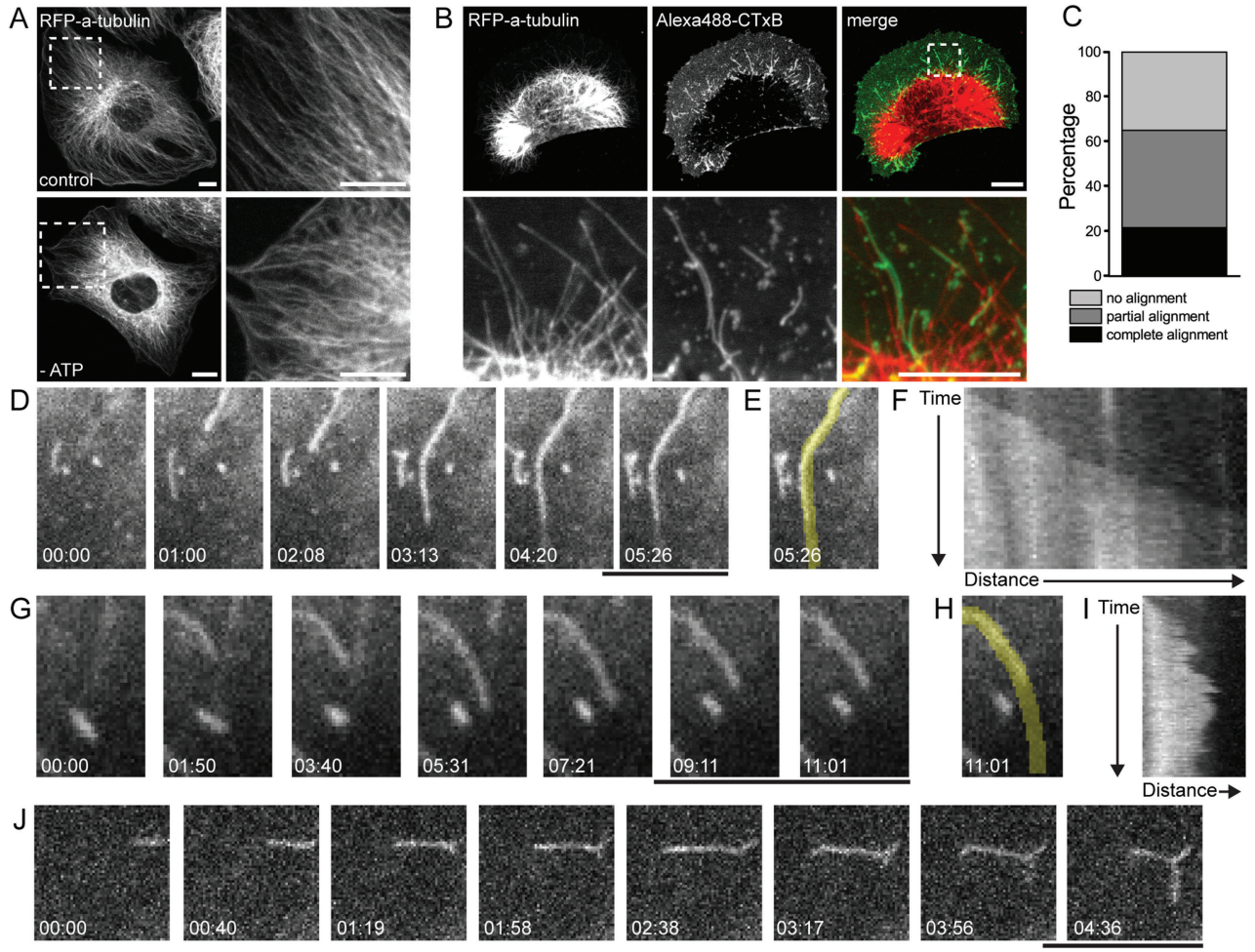

Figure 3: Tubular invaginations align along microtubules and undergo complex motions including bidirectional motility and branching events. A) Microtubules persist in RFP-α-tubulin expressing HeLa cells following ATP depletion. B) CTxB positive invaginations (green) align with taxol-stabilized microtubules (red) in stably expressing RFP-α-tubulin HeLa cells under ATP depletion. C) Percentage of CTxB-positive tubules that align with microtubules (black), partially align with microtubules (gray), or do not colocalize with microtubules (light gray) in ATP-depleted HeLa cells expressing RFP-α-tubulin. $N = 84$ cells. D–J) CTxB-enriched tubules exhibit complex motions in live cells as illustrated by representative frames from time series and corresponding kymographs. Time stamps are in minutes:seconds. D–F) CTxB-positive invaginations often grow in fluid directed motions. G–I) CTxB-positive invaginations also extend, retract and regrow along the same axis. J) Occasionally, the CTxB positive tubules undergo branching events. Bars, 10 μm.

Low levels of microtubule motor activity are retained in ATP-depleted cells

Another way microtubules could support the growth of invaginations would be through the activity of microtubule-based motors (32–34,43). Microtubule-based motility involves two classes of motor proteins, dynein and members of the kinesin family (44,45). Given that the tubular invaginations underwent preferential growth toward the center of the cell, where microtubule minus ends are located (Figure 1, Movies S1 and S2), we hypothesized that the minus-end directed motor dynein might be involved.

Dynein is an ATPase (44) whose activity is expected to be attenuated in ATP-depleted conditions. We thus asked if dynein still functions as a motor in cells depleted of ATP by monitoring the intracellular movement of lysosomes labeled with mCherry-tagged LAMP1 (46).

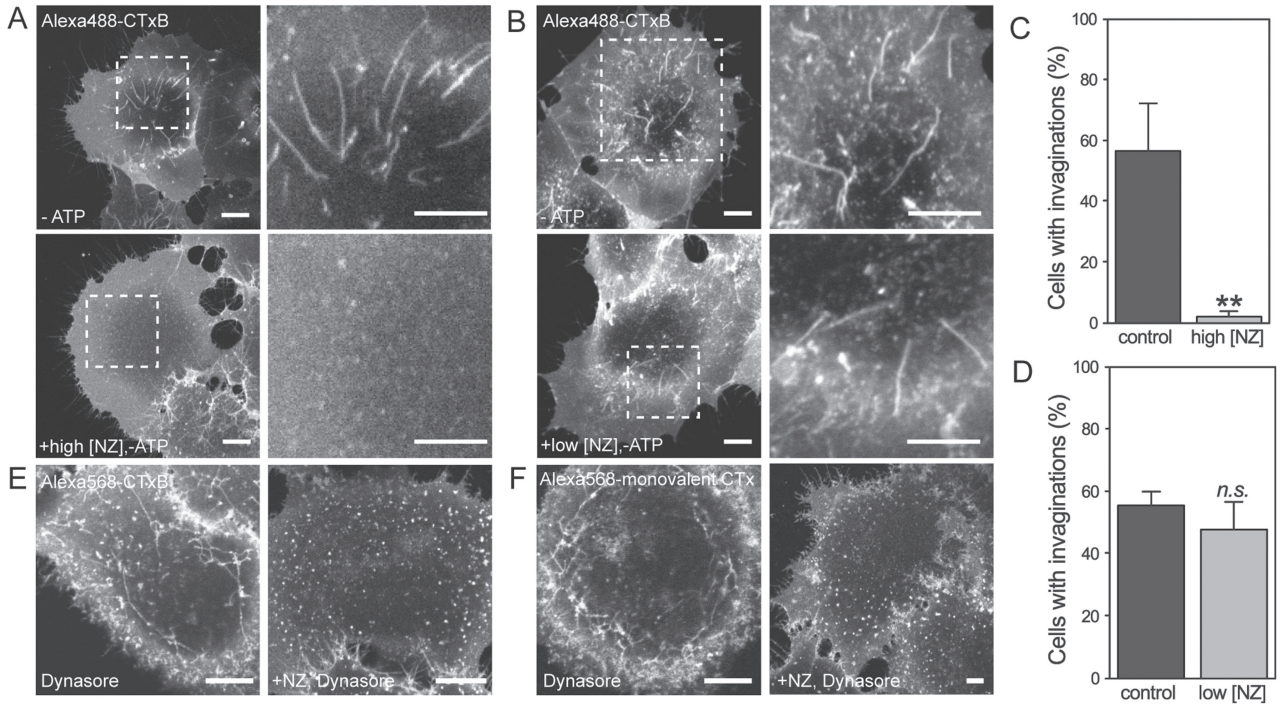

Figure 4: An intact microtubule network is required for the formation of tubular invaginations. A and C) Microtubule disruption with high dose nocodazole prevents the formation of tubular invaginations in ATP-depleted cells (mean ± SD, $N = 74$ cells.) $^{**}p < 0.01$, chi-squared test. B and D) Inhibition of microtubule dynamics with low dose nocodazole has no effect on the formation of tubular invaginations in ATP-depleted cells (mean ± SD, $N = 135–169$ cells.) *n.s.* $p > 0.05$, chi-squared test. E and F) Microtubule disruption prior to Dynasore treatment blocks the formation of branched tubules in cells labeled with either wild type CTxB (E) or monovalent CTx (F). Bars, 10 μm.

Although strongly reduced compared to control cells, some long-range motions of lysosomes persisted in ATP-depleted cells (Figure 5A–G) (Movie S4). These data imply that motor proteins remain active at low levels in ATP-depleted cells, consistent with dynein's known activity under low ATP conditions *in vitro* (47,48).

We also asked whether dynein is localized appropriately to assist with tubule extension. Due to incompatibility of fixation conditions required to preserve dynein staining and tubule morphology, we were unable to determine whether endogenous dynein was present on tubular invaginations. We therefore instead used a HeLa cell line stably expressing low levels of multifunctional green fluorescent protein (mfGFP)-tagged 74-kDa dynein intermediate chain (IC74) (49) to visualize both simultaneously. Some mfGFP-IC74 could be observed at the plasma membrane in ATP-depleted cells, and a few dynein intermediate chain-positive puncta co-localized with the tubular invaginations (Figure S4). These findings further support the possibility that at least a small number of dyneins are localized correctly to facilitate plasma membrane tubulation under these conditions.

The ATPase activity of dynein and an intact dynactin complex are required for tubule extension

To test if dynein contributes to the formation of extended tubular plasma membrane invaginations, we used a small molecule inhibitor of dynein, ciliobrevin A (50). In the presence of ciliobrevin A, we observed impaired formation of tubular invaginations containing CTxB in ATP-depleted cells (Figure 6A,B). This result implicates dynein in the extension of tubular invaginations. To test this hypothesis in another way, we inhibited the function of dynactin, a complex required for dynein function (44,51). We perturbed dynactin by overexpressing either a GFP-tagged form of p50/dynamitin (51) (Figure 6C) or a dsRed-tagged form of the dynein-binding portion of the dynactin subunit

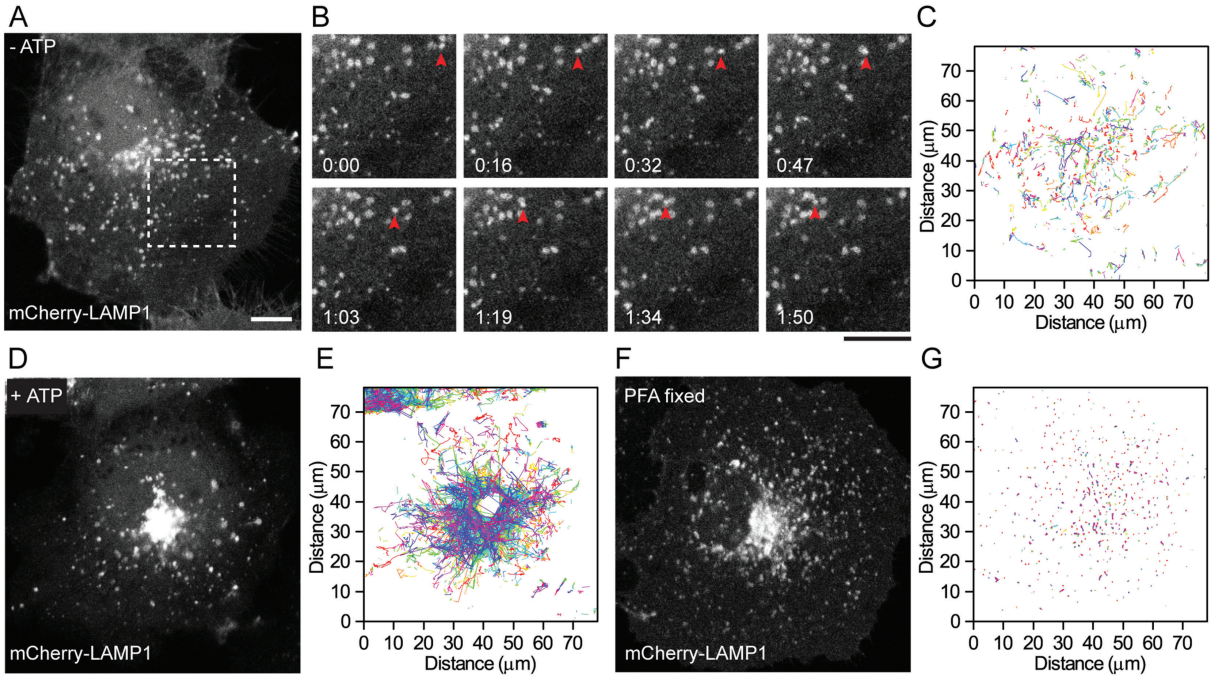

Figure 5: Motor-based motions persist in ATP-depleted cells. A–C) A subset of lysosomes labeled with mCherry-LAMP1 display long range directed motions in ATP-depleted cells. B) Time lapse of zoomed in region of the cell in panel A. An example of a lysosome undergoing long-range directed motion is marked with the arrowhead. C) Tracings of lysosome movement in the cell shown in A. Each track is indicated by a different color. D and E) Frequent long-range directed motions are observed under control conditions. F and G) mCherry-LAMP1 positive lysosomes are immobile in PFA fixed cells. Elapsed time in F, H and J = 470 s. Bars, 10 μm.

p150^{Glued}, CC1-dsRed (51) (Figure 6D,E). Overexpression of either protein strongly inhibited the formation of tubular invaginations in response to ATP depletion (Figure 6C–E). p50 expression also blocked extended branched tubules from forming in Dynasore-treated cells (Figure S3E,F). Thus, dynactin is required for tubulation of the membrane, further implicating dynein as a host cell factor that underlies tubule extension.

Bulk uptake of CTxB is unaffected by disruption of microtubules or the dynactin complex, suggesting the tubular carriers define a low capacity endocytic pathway

Given our findings that microtubules, dynactin and dynein are required for plasma membrane tubulation, we wondered if they are also necessary for the uptake of CTxB. CTxB can be internalized by multiple mechanisms (12,13), including a high capacity pathway that involves morphologically distinct clathrin-independent carriers (16,17) and tubular endocytic intermediates that contain CTxB (13). Interestingly, we found that uptake of CTxB into ATP replete cells was unaffected by the expression of GFP-p50 (Figure 7A,B) or pretreatment of cells with nocodazole (Figure 7C,D). Thus, the microtubule-dependent pathway cannot be highly efficient or high capacity. However, these results do not exclude the possibility that uptake of toxin by plasma membrane tubules is physiologically relevant – as cholera toxin-induced toxicity is poorly correlated with overall levels of toxin internalization (13). Indeed, we found that intact microtubules were required for full toxicity of CTx in polarized human intestinal epithelial T84 cells, as measured by an electrophysiological assay that monitors toxin-induced Cl^- secretion (52) (Figure 7E). This is consistent with a role for microtubules in the uptake or trafficking of CT.

Discussion

Here, we show that microtubules, dynein and dynactin provide an important source of mechanical force that tubulates

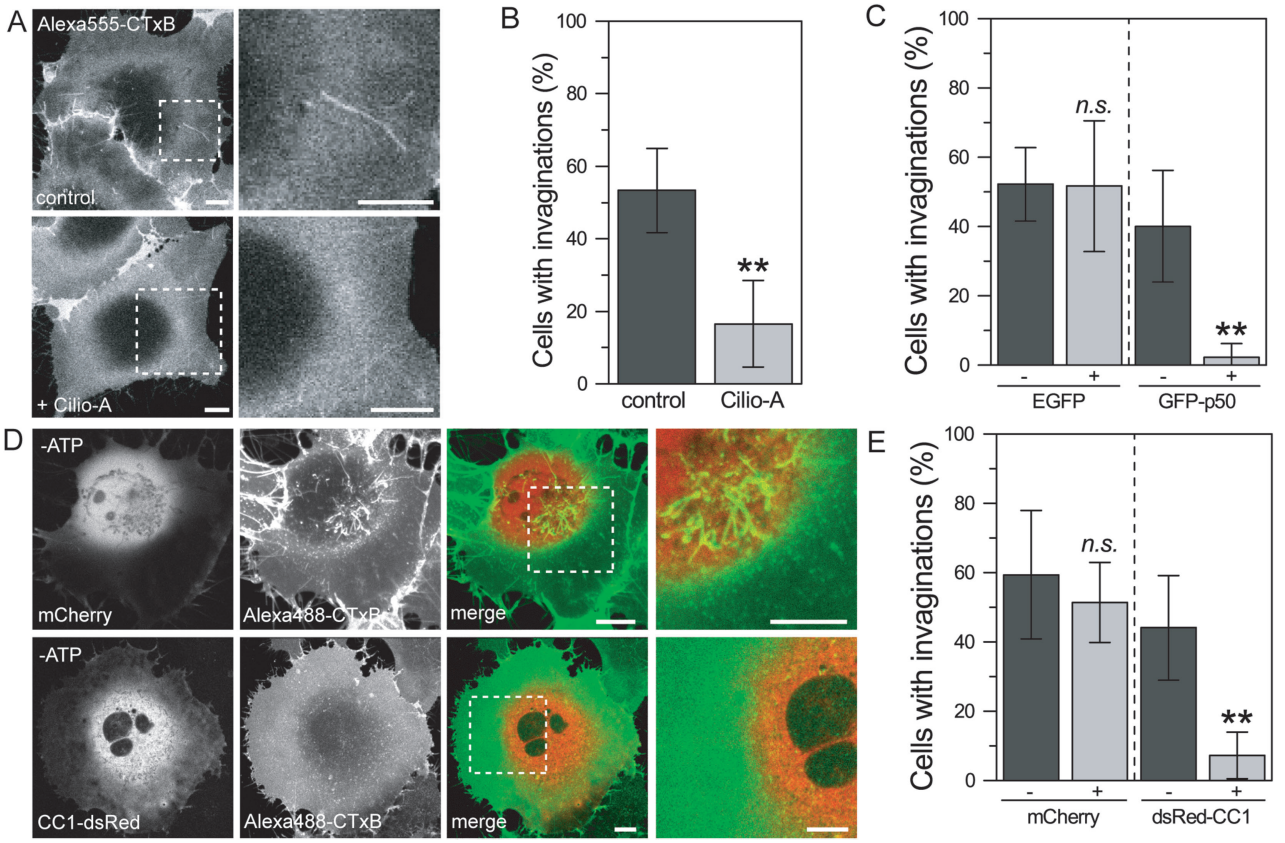

Figure 6: The ATPase activity of dynein and an intact dynactin complex are required for the formation of tubular invaginations. A and B) Inhibition of dynein ATPase activity with ciliobrevin-A (Cilio-A) significantly reduces the percent of cells displaying tubular invaginations (mean ± SD from 95–122 cells). $**p < 0.01$, chi-squared test. C) Expression of GFP-p50 reduced the prevalence of cells with invaginations as compared to untransfected cells (–) or cells expressing EGFP. (mean ± SD from 42–101 cells). *n.s.*, $p > 0.05$; $**p < 0.01$, chi-squared test. D and E) Expression of CC1-dsRed (red) significantly reduces the percent of cells with CTxB positive invaginations (green) as compared to untransfected cells (–) or control cells expressing mCherry (red). (mean ± SD from 40–64 cells). *n.s.*, $p > 0.05$; $**p < 0.01$, chi-squared test. Bars, 10 μm.

the plasma membrane during clathrin-independent endocytosis of CTxB. Interestingly, similar tubules were observed in the presence and absence of bound toxin, suggesting they demarcate an endogenous, toxin-independent pathway. Very recent evidence indicates microtubules and dynein are also involved in the clathrin-independent uptake of STxB via endophilin A2-containing tubules (53). Formation of these endophilin A2-positive tubules is strongly induced by toxin binding (53). Thus, the mechanism of dynein- and microtubule-dependent membrane tubulation that we describe here appears to be a general one utilized by multiple classes of clathrin-independent carriers, inclusive of both constitutive and cargo-induced pathways.

On the basis of our findings, we propose a model wherein dynein and dynactin can interact with the plasma membrane and adjacent microtubules to allow formation and extension of nascent endocytic tubules (Figure 8). Dynein likely drives tubule extension by pulling the membrane along existing microtubules, albeit only slowly under conditions where ATP is limiting as in ATP-depleted cells. Other minus end directed motors, such as kinesins-14 might also contribute to these processes. By providing an internal pulling force that drives membrane curvature, motor-driven bending of the plasma membrane could facilitate recruitment of curvature-sensitive/generating proteins that help stabilize and elongate tubules (54,55). Pulling forces could also participate in other steps in

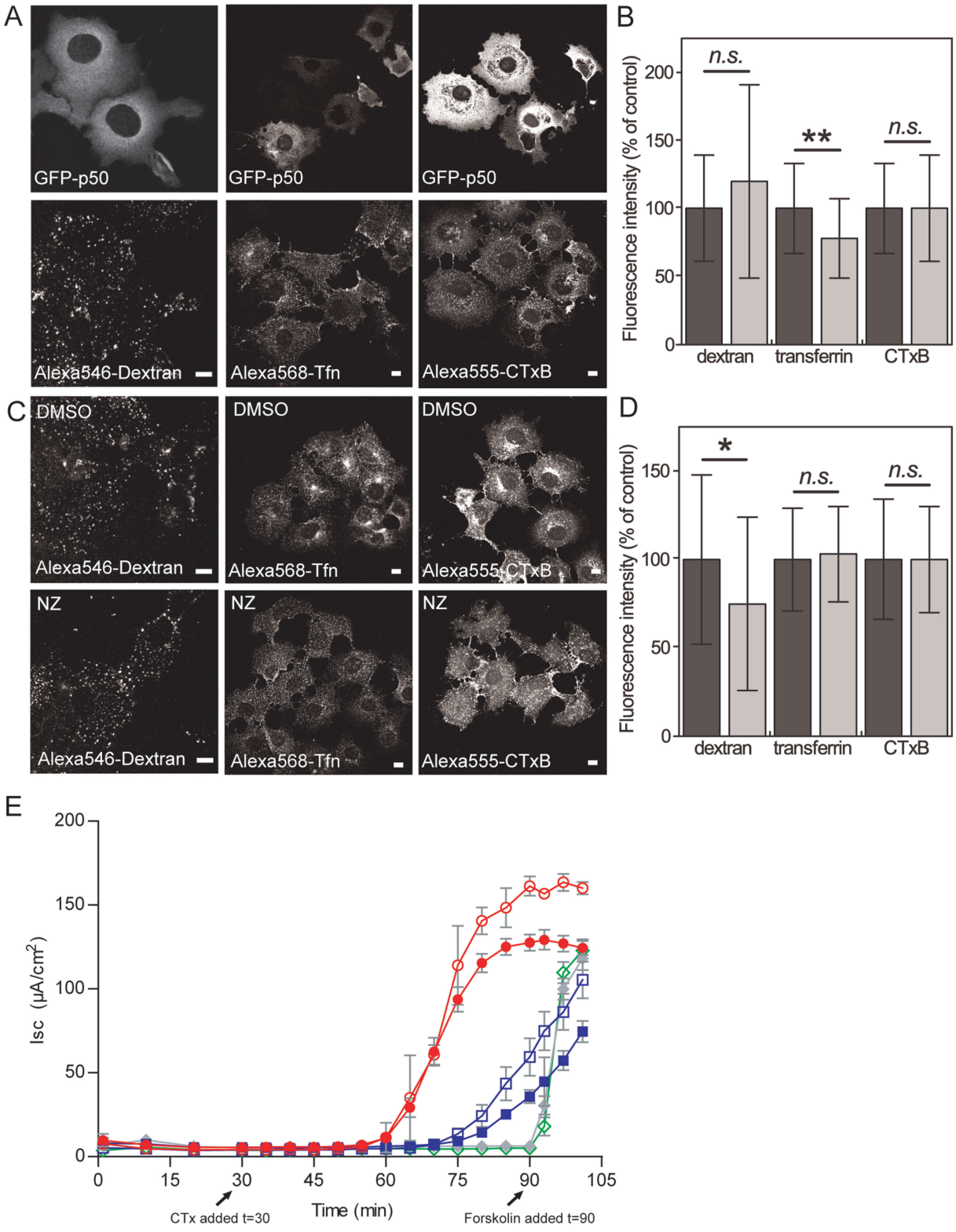

Figure 7: Legend on next page.

clathrin-independent endocytosis. For example, they could help sort cargo into tubules in a curvature-dependent manner (56–58), as well as contribute to the process of membrane scission (53,59).

The exact mechanism by which dynein and dynactin bind the plasma membrane and how this process is regulated in clathrin-independent endocytosis remains to be determined. It could involve recruitment to sites of local membrane bending induced by endogenous cellular factors, similar to that previously described for recruitment of dynein by retromer (56), or in the case of the toxins, by membrane bending at the site of toxin binding as discussed further below (18,30,53). Caveolae could potentially serve as a preferential site for dynein/dynactin recruitment to the plasma membrane, as caveolin-1 has been observed in long, toxin-positive tubules under conditions that inhibit endocytosis (24,60).

The mechanism of attachment of dynein/dynactin to the plasma membrane may alternatively be related to those involved in positioning of the mitotic spindle (61). This scenario seems less likely given that stable anchoring of dynein at the cell cortex is thought to facilitate microtubule-dependent pulling forces (62). Interestingly however, microtubule-dependent plasma membrane invaginations have been reported to form in *C. elegans* embryos at cortical sites where spindle poles are tethered (63). These invaginations are observed at low frequency in unperturbed embryos, but are more readily evident under conditions where the acto-myosin cortex is weakened (63). This suggests that cortical actin reorganization may represent a key event that determines whether microtubule- and dynein-dependent tubulation of the plasma membrane can occur. For example, cortical actin may normally act as a physical barrier between microtubules and the cell surface. Reorganization of cortical actin, either through endogenous processes or in response to actin perturbing agents (64), may permit microtubules access to the plasma membrane, facilitating the formation of the extended tubular carriers into which endocytic cargo such as CTxB enters. Changes in cortical actin organization could also potentially decrease plasma membrane tension, favoring the formation of long invaginations by microtubule-dependent pulling. Actin dynamics may in turn ultimately also contribute to the tubule scission process that releases tubules from the plasma membrane (21,53).

Our findings also have important implications for our understanding of how glycosphingolipid-binding toxins such as cholera toxin and Shiga toxin manipulate cell membranes to facilitate their uptake and subsequent cellular intoxification. It is clear that CTx and STx binding to multiple copies of their glycosphingolipid receptors enhances their toxicity (18,28,29,30,65) and that toxins can induce membrane bending *in vitro* (18,30). Toxin binding can also initiate the recruitment of curvature-sensing proteins to the plasma membrane (53). However, cross-linking of membrane lipids is dispensable for both plasma membrane tubulation (this study) and CTx intoxication of host cells (28,29). While CTxB binding is not required for extended tubular invaginations to form, membrane reorganizations and local bending induced by the AB5 toxins binding to their sphingolipid receptors (18,30) may function cooperatively with the microtubule-based mechanisms of membrane tubulation we propose here. Toxin binding may for example contribute to the induction or

Figure 7: Bulk endocytosis of CTxB is largely unaffected by disruption of microtubules or the dynactin complex. A and B) Endocytosis of dextran, transferrin and CTxB in cells expressing GFP-p50 (gray bars) compared to cells expressing GFP (black bars). B shows mean ± SD for 37–278 cells. *n.s.*, $p > 0.05$, Student's *t*-test. C and D) Effect of microtubule disruption with 5 μg/mL nocodazole (gray bars) on the uptake of dextran, transferrin and CTxB. Control cells were treated with DMSO (black bars). D shows mean ± SD for 78–358 cells. *n.s.*, $p > 0.05$, *, $p < 0.05$, Student's *t*-test. Bars, 10 μm. E) Representative time course of toxin-induced chloride secretion in T84 cells in response to treatment with 20 nM wt CTx. Cells were either pretreated with NZ (closed symbols) or with DMSO (open symbols) prior to toxin addition to either the apical (blue) or basolateral (red) surface at $t = 30$ min as described in the *Materials and Methods*. Forskolin was added to control monolayers (green or gray diamonds) at 90 min in order to demonstrate equivalency of the secretory response and monolayer viability. The error bars indicate the variance calculated as the standard deviation ($n = 3$). Data are representative of the results of two independent experiments.

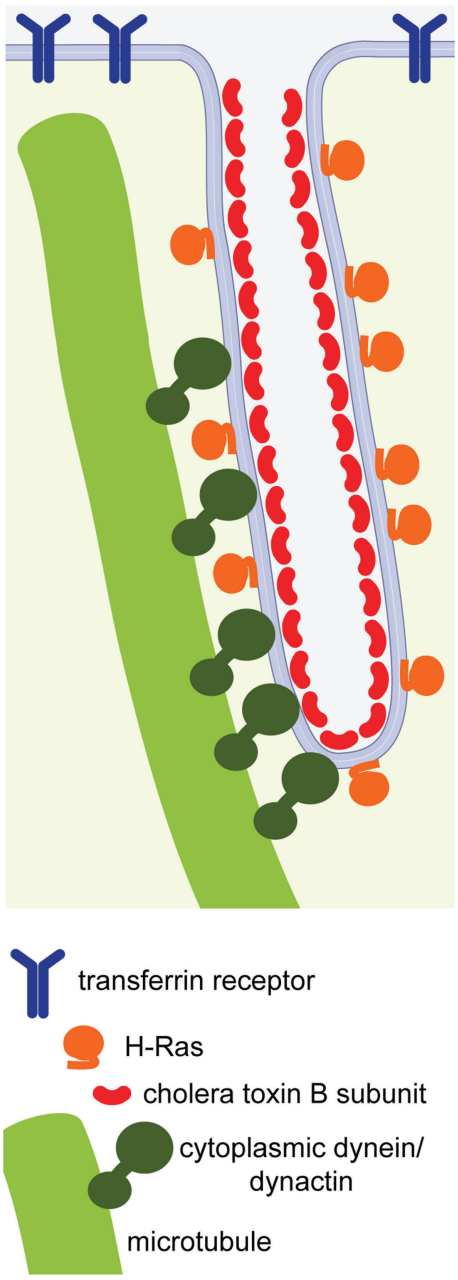

Figure 8: Working model: microtubules, dynactin and cytoplasmic dynein facilitate plasma membrane tubulation. Dynein and dynactin provide attachment sites or generate tugging forces on the plasma membrane, leading to microtubule-dependent tubulation. Glycolipid-binding toxins may further sense, induce or stabilize membrane curvature, enabling their efficient sorting into tubular structures.

stabilization of membrane curvature (53) or favor sorting of the glycosphingolipid-toxin complex into curved structures (66). Indeed, we observed a slight preference of wild type CTxB for sorting into tubules compared to mutant toxins containing only 1 or 2 lipid GM_1 binding sites. Scission of toxin-containing tubules may also depend on cooperative actions of curvature generating proteins and microtubule-based motors (53). Under physiological conditions, STxB and CTxB could also potentially regulate cellular machinery that controls membrane curvature, either by signaling-based mechanisms (67) or by directly influencing microtubule dynamics (68). Still, the cross-linking of membrane glycosphingolipids by toxin is not absolutely required for sorting into tubules or internalization. Our results implicate other mechanisms of membrane tubulation in this pathway, one of which we propose is facilitated by microtubules and the microtubule motor dynein.

Materials and Methods

Cells and reagents

COS-7 and HeLa cells were acquired from ATCC (Manassas, VA). Stable RFP-α-tubulin expressing HeLa cells were a gift from Paul Chang (M.I.T.). HeLa cells stably expressing multifunctional GFP (mfGFP)-tagged 74 kDa dynein intermediate chain (IC74) were kindly provided by Takashi Murayama (Department of Pharmacology, Juntendo University School of Medicine, Tokyo, Japan). T84 cells were cultured as previously described (52). COS-7 cells were maintained in Dulbecco's modified Eagle medium (DMEM) containing 10% fetal bovine serum (Life Technologies) at 37°C and 5% CO_2. HeLa cells were maintained in Roswell Park Memorial Institute medium (RPMI) containing 10% fetal bovine serum at 37°C and 5% CO_2. Media for RFP- α-tubulin HeLa cells additionally contained G418 (Corning), and hygromycin (400 μg/mL) (Invitrogen) was added to media for the IC74 cells. Cells were plated on coverslips or into MatTek chambers (MatTek Corporation) 2 days prior to experiments. Transient transfections were performed 24 h prior to imaging using FuGENE 6 as per manufacturer instructions (Roche Diagnostics).

Alexa488-CTxB and Alexa555-CTxB were obtained from Invitrogen. CTx chimera was generated as previously described (28). Monovalent CTx was made essentially as described (29). Briefly, an *E. coli* expression strain containing three plasmids encoding native CTA, CTB-G33D (non-binding mutant) and C-terminally GS-H6-tagged wt-CTB was induced with 0.0005% L-arabinose and 400 μM IPTG and grown overnight at 30°C. Each subunit is secreted to the periplasm where holotoxins with mixed CTB pentamers assemble from a random assortment of G33D mutant and GS-H6-tagged wt CTB monomers with CTA. This mixture of assembled holotoxins and free B pentamers containing from 0 to 5 GS-H6

tagged B subunits (native binding sites) was purified from a cell extract by Talon affinity chromatography, and separated into individual species by three rounds of ion-exchange chromatography. Free pentamers were first removed by binding to a cationic resin (HS20); the mixture of holotoxins eluting in the unbound fraction was then bound to an HQ20 anion exchange column, and individual species were eluted with a 0–1 M NaCl gradient, peak fractions were pooled, concentrated and repurified by anion exchange. Densitometry of protein bands separated by SDS-PAGE showed the expected ratio of 1 A and 1 tagged wt B subunit to 4 native-sized (G33D) B subunits. Purified holotoxins were stored at 4°C in 50 mM Tris–HCl, pH 8.0. Before labeling, several preparations of single binding site holotoxin were pooled, concentrated and buffer-exchanged into PBS, pH 7.5 by ultrafiltration using an Amicon Ultra-4 (Millipore) 10 K cutoff centrifugal filter.

Alexa568-labeled monovalent CTx was prepared by reacting Alexa568-succinimidyl ester (Invitrogen) to 300 μg toxin chimera (29) in 100 mM sodium bicarbonate buffer pH 8.3 for 1 h under stirring at room temperature and purified using provided size exclusion chromatography resin. Alexa568-labeled wild type CTxB was prepared as above using recombinant B-subunit purified from periplasmic *E. coli* extracts. Alexa 488-STxB and Cy3-STxB along with a plasmid for Gb_3 transferase (69,70) were gifts from Ludger Johannes (Institut Curie).

Plasmids encoding EGFP-HRas, EGFP-HRas-tail (consisting of GFP fused to the C-terminal 10 amino acid residues of HRas), and GFP-Fyn were provided by Mark Philips (NYU School of Medicine) (71); GFP-EB3 (40) was a gift from Anna Akhmanova (Utrecht University); and CC1-dsRed and GFP-p50 (72) were gifts from Trina Schroer (Johns Hopkins). LYFPGT46 (referred to as YFP-GT46) was as previously described (73,74). MyrPalm-mCFP was obtained from Roger Tsien (75).

A plasmid encoding mCherry-LAMP1 was generated by standard techniques by fusing the mammalian expression plasmid for mCherry to DNA encoding rat lysosomal membrane glycoprotein 1 (LAMP1; NM_012857; gift from George Patterson, NIH). A rabbit anti-caveolin-1 antibody was obtained from BD Biosciences. A mouse anti-transferrin receptor antibody was purchased from Life Technologies. A rabbit anti-GFP antibody was obtained from Abcam. An anti-Myc (9B11) mouse monoclonal antibody was from Cell Signaling. Fluorescently labeled secondary antibodies were from Jackson ImmunoResearch and Life Technologies.

D(+)glucose, sodium azide, 2-deoxyglucose, bovine serum albumin (BSA), trichloroacetic acid, Nocodazole (NZ), Dynasore, Latrunculin A, methyl β-cyclodextrin and ciliobrevin A (HPI-4) were purchased from Sigma Aldrich. Taxol was from Alexis Biochemical. HEPES and TAE buffers were purchased from Mediatech, Inc.. Alexa546-dextran was from Life Technologies. Jasplakinolide and Alexa647-transferrin were obtained from Invitrogen.

Confocal microscopy

Confocal microscopy was carried out on a Zeiss LSM 510 confocal microscope (Carl Zeiss MicroImaging, Inc.) using a 40X 1.4 NA Zeiss Plan-Neofluar oil immersion objective or 100X 1.4 NA Zeiss Plan-Apochromat oil immersion objective. Images were collected using 1 Airy unit confocal slices unless otherwise indicated. Cells were maintained in media supplemented with 25 mM HEPES and any indicated drugs as described above for live-cell imaging experiments. Cells were maintained at 37°C using a stage heater and objective heater during imaging. EGFP and Alexa488 were excited using the 488 nm line of a 40 mW Argon laser. YFP was excited using the 514 nm line of the Argon laser. Alexa546, Alexa555, Alexa568, Cy3, RFP and mCherry were excited at 543 nm using a HeNe laser. Alexa647 was excited at 647 nm using a HeNe laser. Fluorescence emission was detected using filter sets provided by the manufacturer. For presentation purposes, images were exported in tiff format and brightness and contrast were adjusted using ImageJ or Fiji (76).

ATP depletion

ATP depletion was performed by pre-incubating cells at 37°C and 5% CO_2 for 15 min in ATP depletion medium, composed of glucose-free DMEM containing 50 mM 2-deoxy-D-glucose, 0.02% sodium azide, 25 mM HEPES, and 1 mg/mL BSA as described in (77). Control cells were incubated in ATP control medium (composed of glucose-free DMEM supplemented with 50 mM D-(+)-glucose, 25 mM HEPES, and 1 mg/mL BSA). Cells were rinsed twice, incubated for 5 min at room temperature with CTxB (100 or 500 nM), STxB (99 nM), CTx chimera (500 nM) or monovalent CTx (400 or 800 nM), rinsed twice, then imaged live at 37°C in either ATP depletion or control media. ATP depletion also induces the formation of abundant actin-rich membrane protrusions (78), so ATP-depleted cells were always imaged in 3-dimensions by confocal microscopy to definitively identify invaginations (Figure S1). For some experiments, cells were pretreated with Jasplakinolide (250 nM) for 30 min prior to ATP depletion, then imaged in the continued presence of both Jasplakinolide and ATP depletion medium.

Quantification of cellular ATP levels

ATP depletion was verified to decrease ATP levels to <5% of control values using the commercially available ENLITEN® ATP assay kit (Promega). For this assay, COS-7 cells were split into 12 well plates. After 2 days the medium was removed and some cells were incubated directly in 500 μL ATP-extraction solution [1% TCA in Tris-Acetate-EDTA (TAE) buffer] to collect baseline ATP readings. The remaining cells were rinsed twice with ATP depletion media and incubated at 37°C and 5% CO_2. At the indicated times after the initiation of ATP depletion, the depletion media was replaced with 500 μL ATP-extraction solution. Cells were incubated in ATP-extraction solution for 30 min at RT, as described before (79). Aliquots of the cell extract were then moved to 96 well plates and diluted tenfold in TAE buffer. Reaction reagent containing luciferase was added to each well and the chemiluminescence was read on a Synergy H4 Hybrid Multi-Mode Microplate Reader (BioTek).

Actin disruption

To disrupt actin, cells were first washed with imaging buffer, incubated for 5 min in 1 μM Alexa546-CTxB in imaging buffer, and washed again.

Actin depolymerization was then performed by incubating the cells at 37°C for 5 min in imaging buffer containing 1 μM Latrunculin A. Control cells were incubated in imaging buffer containing 0.1% DMSO. Cells were maintained in their respective buffer during imaging and all imaging was performed within 30 min of treatment. Where indicated, cells were preincubated with 5 μg/mL NZ for 15 min on ice, followed by a 1 h incubation at 37°C prior to Latrunculin A treatment and CTxB labeling, then imaged live in the continued presence of both Latrunculin A and NZ.

Actin stabilization

Cell culture media was replaced with complete imaging buffer containing 250 nM Jasplakinolide or DMSO and incubated at 37°C and 5% CO_2 for 30 min. Cells were then labeled with 100 nM Alexa-labeled CTxB for 5 min at RT in complete imaging buffer containing 250 nM Jasplakinolide or DMSO. Cells were rinsed and imaged in complete imaging buffer containing 250 nM Jasplakinolide or DMSO. Where indicated, cells were ATP depleted following Jasplakinolide treatment as described above. In some experiments, cells were preincubated with 5 μg/mL NZ for 15 min on ice followed by a 1 h incubation at 37°C prior to Jasplakinolide treatment and CTxB labeling, then imaged live in the continued presence of both Jasplakinolide and NZ.

Dynamin inhibition

Dynamin 2 was inhibited using the small molecule inhibitor, Dynasore (80). Cell culture media was replaced with DMEM supplemented with 25 μM HEPES and either 80 μM Dynasore or DMSO. Cells were incubated in Dynasore or DMSO at 37°C and 5% CO_2 for 30 min. Cells were then labeled with either 100 nM Alexa568-CTxB or 400–800 nM Alexa568 monovalent CTx for 5 min at RT, rinsed and imaged in DMEM supplemented with 25 μM HEPES and either 80 μM Dynasore or DMSO. Where indicated, cells were preincubated with 5 μg/mL NZ for 15 min on ice followed by a 1 h incubation at 37°C prior to Dynasore treatment and CTxB or monovalent CTx labeling, then imaged live in the continued presence of both Dynasore and NZ. In other experiments, cells were transfected with GFP or GFP-p50 prior to Dynasore treatment and toxin labeling as described above, then imaged live.

Analysis of surface accessibility of tubules

ATP depleted COS-7 were labeled with 25 nM Alexa555-CTxB and placed on the stage at 37°C. A highly concentrated dose of Alexa488-CTxB was added to bring the final Alexa488-CTxB concentration in the imaging buffer to 50 nM while continuously imaging.

Immunofluorescence labeling

For immunostaining of caveolin-1 and transferrin receptor, cells grown in MatTek dishes were subjected to ATP depletion and labeled with CTxB as described above. After CTxB labeling they were incubated for 30 min 37°C and 5% CO_2 in the continued presence of the ATP depletion media. They were then fixed at 37°C with 4% PFA/0.2% glutaraldehyde for 15 min. After rinsing several times they were blocked in PBS containing 10% FBS and 0.1% saponin for 15 min and then labeled with transferrin receptor or caveolin-1 antibodies for 30 min. They were again washed and then labeled with secondary antibody for 30 min. After several additional washes they were imaged.

In IC74 cells, immunolabeling of the tagged dynein intermediate chain subunit was performed using an anti-myc antibody in order to amplify the fluorescence signal. For these experiments, cells grown on coverslips were either ATP depleted for 15 min or left untreated. They were then rinsed twice and incubated for 5 min at room temperature with 100 nM Alexa488-CTxB or Alexa555-CTxB. The cells were then rinsed twice and fixed at 37°C for 15 min in pre-warmed 4% PFA/0.2% glutaraldehyde. Post fixation, the cells were quenched by three rinses in 100 mM glycine in PBS. Permeabilization and blocking for 60 min at RT was performed in blocking buffer composed of 0.1% TX-100 in PBS containing 5% glycine and 5% normal goat or donkey serum. Cells were incubated with rabbit anti-myc antibody for 2 h at RT. After rinsing in PBS coverslips were incubated for 1 h in a 1:200 dilution of fluorescently-conjugated secondary antibodies, and mounted using ProLong Gold (Invitrogen, Carlsbad, CA).

Microtubule stabilization

HeLa cells expressing RFP-α-tubulin were incubated with imaging buffer containing 1 μM taxol for 4 h at 37°C. They were then rinsed twice with ATP depletion media containing 1 μM taxol, incubated at 37°C for 15 min, labeled with 100 nM Alexa-labeled CTxB for 5 min at RT, rinsed and imaged in ATP depletion media containing 1 μM taxol.

Suppression of microtubule plus end dynamics

Cells were incubated with imaging buffer containing 150 nM NZ (40–42) or DMSO at 37°C for 5 min. The media was then replaced with ATP depletion media supplemented with 150 nM NZ or DMSO and incubated at 37°C for 15 min. Cells were labeled with 100 nM Alexa-labeled CTxB for 5 min at RT, rinsed and imaged in ATP depletion media containing 150 nM NZ or DMSO.

Microtubule disruption

To disrupt microtubules, cells were incubated with imaging buffer (phenol red-free DMEM, 10% BSA, 25 mM HEPES, and 1 mg/mL BSA) containing 5 μg/mL (16.7 μM) NZ (81,82) or DMSO on ice for 15 min. Cells were then shifted to 37°C for 1 h and subjected to further drug treatments and CTx or CTxB labeling as indicated above. Cells were imaged in the continued presence of either NZ or DMSO. The efficacy of microtubule disruption was confirmed by visualizing the distribution of tubulin in control experiments.

Analysis of fluid phase and transferrin uptake in ATP-depleted cells

Control experiments were carried out to verify the efficacy of ATP depletion by testing its effects on fluid phase and transferrin uptake (Figure S1). For the fluid phase uptake experiments, COS-7 cells were preincubated in ATP control media or ATP depletion media for 15 min. They were then labeled with 100 nM Alexa488-CTxB (to mark the position of cells) and

Alexa546-Dextran (1 mg/mL) for 20 min at 37°C, rinsed 10 times with the respective media and imaged live. To measure transferrin uptake in ATP-depleted cells, cells were serum starved for 1 h prior to incubation in ATP control media or ATP depletion media for 15 min. They were then labeled with 100 nM Alexa488-CTxB (to mark the position of cells) and 25 μg/mL Alexa647 transferrin for 20 min at 37°C, rinsed 5 times with respective media, and imaged live.

Inhibition of dynein motor activity

In control experiments, we defined conditions in which ciliobrevin A inhibited the dynein-based delivery of CTxB to the perinuclear region in cells with physiological levels of ATP (Figure S3C,D). To generate ciliobrevin A dose dependence curves, ciliobrevin A was diluted in DMSO and stocks were produced by serial dilution in DMEM + 10% fetal bovine serum. Cells were incubated in medium containing ciliobrevin A or DMSO at 37°C for 1 h. They were then labeled with 100 nM Alexa-labeled CTxB in ciliobrevin A or DMSO containing media for 5 min at RT, rinsed and either fixed immediately or shifted to 37°C and 5% CO_2 for 30 min prior to fixation with 3.4% PFA at RT for 15 min. Samples were mounted in ProLong Gold (Invitrogen, Carlsbad, CA) and fields of cells were imaged and image analysis performed as indicated below.

For experiments examining the effects of ciliobrevin A on tubule formation, cell culture media was replaced with imaging buffer containing 500 μM ciliobrevin A or DMSO and incubated at 37°C and 5% CO_2 for 1 h. Cells were rinsed twice with ATP depletion or control media containing ciliobrevin A or DMSO and incubated at 37°C and 5% CO_2 for 15 min. Cells were labeled with 100 nM Alexa-labeled CTxB for 5 min at RT, rinsed and imaged in ATP depletion or control media containing ciliobrevin A or DMSO. Care was taken to protect ciliobrevin-A from light throughout experiment.

Analysis of fluid phase uptake in cells expressing GFP-p50

COS-7 cells transiently expressing EGFP or EGFP-p50 were loaded with Alexa-546 dextran (1 mg/mL) in 100 μL of serum free imaging buffer and incubated at 37°C for 20 min, rinsed with imaging buffer 10 times and imaged live. Images were collected using a 1 Airy unit confocal slice under identical imaging conditions for cells expressing EGFP and EGFP-p50.

Analysis of transferrin and CTxB uptake in cells expressing GFP-p50

COS-7 cells plated on cover slips were transfected with EGFP or GFP-p50. To quantify the cellular uptake of CTxB, cells were rinsed with cold imaging buffer and labeled with 100 nM A555-CTxB for 5 min on ice. For quantification of transferrin uptake, cells were serum starved using DMEM containing 25 mM HEPES for 1 h at 37°C and 5% CO_2. Serum starved cells were then rinsed with cold DMEM supplemented with 10% FBS and 25 mM HEPES and labeled with 5 μg/mL Alexa568-transferrin for 5 min on ice. Cells were rinsed with imaging buffer and shifted to 37°C and 5% CO_2 for 20 min. Acid stripping was performed on ice by incubating cells with 2 mL of 100 mM glycine, pH 2.0, for 5 min and then with HBSS, pH 7.4, for 5 min. Acid-stripped samples were subsequently incubated with 37°C HBSS, pH 7.4, for 10 s to promote release of remaining surface-bound toxin or transferrin (83). This process was repeated 3 times. Cells were fixed in 3.4% PFA at room temperature for 15 min and rinsed with 1x PBS. Cells were labeled with an anti-GFP primary antibody and an Alexa488 secondary antibody. Samples were mounted in ProLong Gold. Cells were imaged at 1x zoom and multiple fields were collected using a 1 Airy unit confocal slice for CTxB and a 2 Airy unit slice for transferrin. Experiments were performed at least three times.

Analysis of fluid phase uptake in NZ-treated cells

COS-7 cells were transiently transfected with EGFP (to mark the position of cells) the day before the experiment. The next day, cells were pre-chilled on ice in serum free imaging buffer for 5 min, then incubated with serum free imaging buffer containing 5 μg/mL (16.7 μM) NZ or DMSO on ice for 15 min. Cells were then shifted to 37°C for 1 h. They were then labeled with Alexa546 dextran (1 mg/mL) for 20 min at 37°C in the continued presence of NZ or DMSO, rinsed 10 times with the respective media and imaged live. Images were collected using a 1 Airy unit slice under identical imaging conditions for the NZ and DMSO-treated samples.

Analysis of transferrin and CTxB uptake in NZ-treated cells

COS-7 cells were transiently transfected with EGFP (to mark the position of cells) the day before the experiment. The next day, cells were pre-chilled on ice in serum free imaging buffer for 5 min, then incubated with serum free imaging buffer containing 5 μg/mL (16.7 μM) NZ or DMSO on ice for 15 min. Cells were then shifted to 37°C for 1 h. Cells were then labeled with either CTxB or transferrin exactly as described above except that NZ or DMSO were included in all labeling and washing steps. Acid stripping and further processing of cells was performed exactly as described above.

Electrophysiology

Measurements of short circuit currents (Isc) and resistance (R) were performed on confluent monolayers of human intestinal T84 cells grown on 0.33 cm^2 filters, as previously described (52). Monolayers were treated with 5 μg/mL nocodazole or DMSO for 30 min on ice followed by further incubation for 30 min at 37°C prior to addition of 20 nM cholera toxin.

Image analysis

To quantify the percentage of a population of ATP-depleted cells containing invaginations, full field (512 × 512) *z*-stacks of fields of cells were taken at 1.7× zoom on a 40× objective, with line averaging of 4 and optimal overlay in *z*-direction. *z*-Stacks were collected consecutively for 50 min after labeling with toxin. Cells were then scored by hand as displaying or not displaying invaginations. For cells expressing a plasmid, that is CC1-dsRed, the cells were scored in the CTxB channel with the experimentalist blind to which cells were expressing the plasmid and which were not.

To determine the number and length of invaginations *z*-sections were taken of individual ATP-depleted cells consecutively for 50 min after labeling with toxin. The JFilament plugin (Dimitrios Vavylonis and Xiaolei Huang; Lehigh University) for ImageJ was used to trace individual invaginations in 2D. The automated snake tracking feature was used to align the snakes with the invaginations. Tracings were examined and corrected by hand. Kymographs were produced using the MultipleKymograph plugin for ImageJ.

To quantify the effects of ATP depletion, NZ treatment and GFP-p50 expression on the uptake of endocytic cargo, outlines of cells were made in the GFP or CTxB channel using ImageJ. The average fluorescence intensity in the endocytic cargo channel was then recorded from the same regions. Background fluorescence was measured from regions devoid of cells. After subtracting background, the data were normalized to 100% of control values.

For lysosomal tracking experiments, particle detection was performed using a custom-written MATLAB algorithm (available upon request) and tracking was performed using u-track 2.0 software (http://lccb.hms.harvard.edu/software.html) (84). Both programs were run using MATLAB 7.11.0 (Mathworks).

The ciliobrevin A dose dependence curve was generated by collecting full field (512 × 512) 16 bit images using a 40x objective with line averaging of 8. ROIs were then drawn around the perinuclear space, flat membrane regions and background in ImageJ. Perinuclear and membrane per pixel fluorescence were corrected for background fluorescence and then divided to produce a perinuclear to membrane ratio per cell.

Statistical analysis

All experiments were performed at least twice and most were carried out three or more times. Chi-square tests were performed using Excel (Microsoft), and Student t-tests were performed using Excel or OriginPro 8.6 (OriginLab).

Acknowledgments

We thank Dana Hardbower, Carol Landerman and Bradley Clarke for assistance with experiments; Drs. Ludger Johannes, Ramiro Massol, Irina Kaverina, Julie Donaldson, Mark McNiven, Stephen King and Puck Ohi for stimulating discussions; Dr. Aurelio Galli for comments on the manuscript; Jacob Dowler for assistance with figure preparation; and all those who contributed reagents. Supported by NIH R01 GM106720 (AKK), NIH RO1 GM073846 (AKK), R01 HL111259 (AKK), NIH RO1 AI31940 (RKH), NIH R01 GM44589 (TAS), NIH grants DK48106, DK084424 and DK090603 and the Harvard Digestive Diseases Center P30 DK34854 (WIL), the Vanderbilt Molecular Biophysics training grant (NIH T32 GM08320) (CAD), a Vanderbilt Discovery Grant (Dr. Todd Graham and AKK), and NIH grant R44-EB008589 (to J. Damiano). It also utilized the core(s) of the Vanderbilt Diabetes Research and Training Center funded by grant DK020593 from the National Institute of Diabetes and Digestive and Kidney Disease. MWD was supported by the National High Magnetic Field Laboratory, which is supported by NSF DMR-1157490 and the State of Florida. The funding sources had no role in the study design, collection, analysis or interpretation of data, writing the report or the decision to submit the paper for publication.

Supporting Information

Additional Supporting Information may be found in the online version of this article:

Figure S1: Control experiments characterizing the properties of the tubular invaginations and documenting the efficacy of ATP depletion. ATP depletion impairs clathrin-dependent and -independent endocytosis, resulting in the accumulation of STxB and CTxB in plasma membrane tubular invaginations. A) Alexa488-STxB and Alexa488-CTxB accumulate in tubular invaginations in ATP depleted COS-7 cells. To facilitate STxB labeling, cells were transfected with Gb_3 synthase. B and C) As reported previously (78), fluorescent CTxB labels both plasma membrane invaginations (arrowheads) and plasma membrane protrusions (arrows) in ATP-depleted cells. B and C are single frames from a confocal *z*-stack. Dashes mark the position of the *xz*-sections shown below. D) Alexa488-STxB and Alexa555-CTxB colocalize in invaginations in ATP depleted COS-7 cells expressing Gb_3 synthase. E) Tubules prelabeled with Alexa555-CTxB filled at approximately the same rate as newly added Alexa488-CTxB accumulates at the plasma membrane, indicating that the tubules are open to the fluid phase in ATP-depleted cells. Time stamps are in minutes:seconds. F–H) ATP depletion inhibits uptake of dextran and internalization of transferrin (Tfn) (Mean ± SD, $N = 325–417$ cells). ***, $p < 0.001$, Student's *t*-test. Bars, 10 µm. (Related to Figure 1.)

Figure S2: Plasma membrane derived tubules are selective for membrane markers. A and B) CFP-Myr-palm and GFP-Fyn accumulate in tubular invaginations in either the (A) presence or (B) absence of CTxB in ATP-depleted cells, whereas YFP-GT46 is excluded from tubules. C and D) Endogenous transferrin receptor (C) and caveolin-1 (D) typically did not colocalize with tubules in immunostained ATP-depleted cells, although occasionally caveolin-1 staining was seen at the end of a tubule (arrowhead). (Related to Figure 2)

Figure S3: Invaginations present following Lat A, Jasplak, or Dynasore treatment are dependent on microtubules and dynein. A and B) Pretreatment of cells with 16.6 µM nocodazole prior to LatA (A) or Jasplakinolide treatment (B) blocks tubule formation. C and D) Pretreatment with ciliobrevin A (Cilio-A) disrupts delivery of CTxB to perinuclear compartments in ATP replete cells in a dose-dependent manner. $n = 36–108$ cells; error bars = SD. E and F) Expression of GFP-p50 (E), but not GFP alone (F) blocked the formation of long branched tubules in Dynasore-treated cells. Similar results were obtained for both wild type CTxB or monovalent CTx. Bars, 10 µm. (Related to Figures 4 and 6)

Figure S4: Some dynein is associated with the tubular invaginations. A) Distribution of mfGFP-dynein 74 kDa intermediate chain in a stably expressing HeLa cell line. Cells were fixed and immunostained using

a myc antibody to enhance the fluorescence signal. B) Following ATP depletion, dynein 74 kDa intermediate chain staining is apparent at the plasma membrane (arrowheads). C) mfGFP-IC74 expressing cells were ATP depleted, labeled with CTxB, fixed and immunostained for tagged dynein intermediate chain. D) Zoom of boxed region of cell shown in C. Some mfGFP-IC74-positive puncta align along CTxB-containing tubular invaginations. Bars, 5 μm. (Related to Figure 5)

Movie S1: Dynamics of growth of CTxB-positive tubular invaginations in ATP depleted COS-7 cells. Correspond to cells shown in Figure 3. Time stamps are in minutes:seconds. Bar, 10 μm. (Related to Figure 3).

Movie S2: Dynamics of growth of CTxB-positive tubular invaginations in ATP depleted COS-7 cells. Correspond to cells shown in Figure 3. Time stamps are in minutes:seconds. Bar, 10 μm. (Related to Figure 3).

Movie S3: EB3-GFP is not enriched at microtubule plus ends in ATP-depleted cells. Time stamps are in minutes:seconds. Bar, 10 μm. (Related to Figure 4).

Movie S4: ATP depletion attenuates, but does not completely eliminate the directed motions of mCherry-LAMP-1 positive structures compared to control conditions. Corresponds to cells shown in Figure 4. Time stamps are in minutes:seconds. Bar, 10 μm. (Related to Figure 5).

References

1. McMahon HT, Boucrot E. Molecular mechanism and physiological functions of clathrin-mediated endocytosis. Nat Rev Mol Cell Biol 2011;12:517–533.
2. Sandvig K, Pust S, Skotland T, van Deurs B. Clathrin-independent endocytosis: mechanisms and function. Curr Opin Cell Biol 2011;23:413–420.
3. Doherty GJ, McMahon HT. Mechanisms of endocytosis. Annu Rev Biochem 2009;78:857–902.
4. Howes MT, Mayor S, Parton RG. Molecules, mechanisms, and cellular roles of clathrin-independent endocytosis. Curr Opin Cell Biol 2010;22:519–527.
5. Mayor S, Pagano RE. Pathways of clathrin-independent endocytosis. Nat Rev Mol Cell Biol 2007;8:603–612.
6. Kumari S, Mg S, Mayor S. Endocytosis unplugged: multiple ways to enter the cell. Cell Res 2010;20:256–275.
7. Hansen CG, Nichols BJ. Molecular mechanisms of clathrin-independent endocytosis. J Cell Sci 2009;122:1713–1721.
8. Donaldson JG, Porat-Shliom N, Cohen LA. Clathrin-independent endocytosis: a unique platform for cell signaling and PM remodeling. Cell Signal 2009;21:1–6.
9. Mayor S, Parton RG, Donaldson JG. Clathrin-independent pathways of endocytosis. Cold Spring Harb Perspect Biol 2014;6:a016758.
10. Pang H, Le PU, Nabi IR. Ganglioside GM1 levels are a determinant of the extent of caveolae/raft-dependent endocytosis of cholera toxin to the Golgi apparatus. J Cell Sci 2004;117:1421–1430.
11. Parton RG. Ultrastructural localization of gangliosides; GM1 is concentrated in caveolae. J Histochem Cytochem 1994;42:155–166.
12. Torgersen ML, Skretting G, van Deurs B, Sandvig K. Internalization of cholera toxin by different endocytic mechanisms. J Cell Sci 2001;114:3737–3747.
13. Massol RH, Larsen JE, Fujinaga Y, Lencer WI, Kirchhausen T. Cholera toxin toxicity does not require functional Arf6- and dynamin-dependent endocytic pathways. Mol Biol Cell 2004;15:3631–3641.
14. Glebov OO, Bright NA, Nichols BJ. Flotillin-1 defines a clathrin-independent endocytic pathway in mammalian cells. Nat Cell Biol 2006;8:46–54.
15. Lundmark R, Doherty GJ, Howes MT, Cortese K, Vallis Y, Parton RG, McMahon HT. The GTPase-activating protein GRAF1 regulates the CLIC/GEEC endocytic pathway. Curr Biol 2008;18:1802–1808.
16. Howes MT, Kirkham M, Riches J, Cortese K, Walser PJ, Simpson F, Hill MM, Jones A, Lundmark R, Lindsay MR, Hernandez-Deviez DJ, Hadzic G, McCluskey A, Bashir R, Liu L, et al. Clathrin-independent carriers form a high capacity endocytic sorting system at the leading edge of migrating cells. J Cell Biol 2010;190:675–691.
17. Kirkham M, Fujita A, Chadda R, Nixon SJ, Kurzchalia TV, Sharma DK, Pagano RE, Hancock JF, Mayor S, Parton RG. Ultrastructural identification of uncoated caveolin-independent early endocytic vehicles. J Cell Biol 2005;168:465–476.
18. Römer W, Berland L, Chambon V, Gaus K, Windschiegl B, Tenza D, Aly MR, Fraisier V, Florent JC, Perrais D, Lamaze C, Raposo G, Steinem C, Sens P, Bassereau P, et al. Shiga toxin induces tubular membrane invaginations for its uptake into cells. Nature 2007;450:670–675.
19. Chinnapen DJ, Chinnapen H, Saslowsky D, Lencer WI. Rafting with cholera toxin: endocytosis and trafficking from plasma membrane to ER. FEMS Microbiol Lett 2007;266:129–137.
20. Badizadegan K, Wolf AA, Rodighiero C, Jobling M, Hirst TR, Holmes RK, Lencer WI. Floating cholera toxin into epithelial cells: functional association with caveolae-like detergent-insoluble membrane microdomains. Int J Med Microbiol 2000;290:403–408.
21. Römer W, Pontani LL, Sorre B, Rentero C, Berland L, Chambon V, Lamaze C, Bassereau P, Sykes C, Gaus K, Johannes L. Actin dynamics drive membrane reorganization and scission in clathrin-independent endocytosis. Cell 2010;140:540–553.
22. Nichols BJ, Kenworthy AK, Polishchuk RS, Lodge R, Roberts TH, Hirschberg K, Phair RD, Lippincott-Schwartz J. Rapid cycling of lipid raft markers between the cell surface and Golgi complex. J Cell Biol 2001;153:529–541.
23. Nichols BJ. A distinct class of endosome mediates clathrin-independent endocytosis to the Golgi complex. Nat Cell Biol 2002;4:374–378.
24. Hansen CG, Bright NA, Howard G, Nichols BJ. SDPR induces membrane curvature and functions in the formation of caveolae. Nat Cell Biol 2009;11:807–814.
25. de Kreuk BJ, Nethe M, Fernandez-Borja M, Anthony EC, Hensbergen PJ, Deelder AM, Plomann M, Hordijk PL. The F-BAR domain protein PACSIN2 associates with Rac1 and regulates cell spreading and migration. J Cell Sci 2011;124:2375–2388.

26. Pina DG, Johannes L. Cholera and Shiga toxin B-subunits: thermodynamic and structural considerations for function and biomedical applications. Toxicon 2005;45:389–393.
27. Wernick NL, Chinnapen DJ, Cho JA, Lencer WI. Cholera toxin: an intracellular journey into the cytosol by way of the endoplasmic reticulum. Toxins (Basel) 2010;2:310–325.
28. Wolf AA, Jobling MG, Saslowsky DE, Kern E, Drake KR, Kenworthy AK, Holmes RK, Lencer WI. Attenuated endocytosis and toxicity of a mutant cholera toxin with decreased ability to cluster GM1. Infect Immun 2008;76:1476–1484.
29. Jobling MG, Yang Z, Kam WR, Lencer WI, Holmes RK. A single native ganglioside GM1-binding site is sufficient for cholera toxin to bind to cells and complete the intoxication pathway. MBio 2012;3:e00401–e00412.
30. Ewers H, Römer W, Smith AE, Bacia K, Dmitrieff S, Chai W, Mancini R, Kartenbeck J, Chambon V, Berland L, Oppenheim A, Schwarzmann G, Feizi T, Schwille P, Sens P, et al. GM1 structure determines SV40-induced membrane invagination and infection. Nat Cell Biol 2010;12:11–18; sup pp 11–12.
31. Johannes L, Mayor S. Induced domain formation in endocytic invagination, lipid sorting, and scission. Cell 2010;142:507–510.
32. Anitei M, Hoflack B. Bridging membrane and cytoskeleton dynamics in the secretory and endocytic pathways. Nat Cell Biol 2012;14:11–19.
33. Stephens DJ. Functional coupling of microtubules to membranes - implications for membrane structure and dynamics. J Cell Sci 2012;125:2795–2804.
34. Leduc C, Campas O, Joanny JF, Prost J, Bassereau P. Mechanism of membrane nanotube formation by molecular motors. Biochim Biophys Acta 2010;1798:1418–1426.
35. Vaughan KT. Surfing, regulating and capturing: are all microtubule-tip-tracking proteins created equal? Trends Cell Biol 2004;14:491–496.
36. Mimori-Kiyosue Y, Tsukita S. "Search-and-capture" of microtubules through plus-end-binding proteins (+TIPs). J Biochem 2003;134:321–326.
37. Vaughan PS, Miura P, Henderson M, Byrne B, Vaughan KT. A role for regulated binding of p150(Glued) to microtubule plus ends in organelle transport. J Cell Biol 2002;158:305–319.
38. Lomakin AJ, Semenova I, Zaliapin I, Kraikivski P, Nadezhdina E, Slepchenko BM, Akhmanova A, Rodionov V. CLIP-170-dependent capture of membrane organelles by microtubules initiates minus-end directed transport. Dev Cell 2009;17:323–333.
39. Waterman-Storer CM, Salmon ED. Endoplasmic reticulum membrane tubules are distributed by microtubules in living cells using three distinct mechanisms. Curr Biol 1998;8:798–806.
40. Stepanova T, Slemmer J, Hoogenraad CC, Lansbergen G, Dortland B, De Zeeuw CI, Grosveld F, van Cappellen G, Akhmanova A, Galjart N. Visualization of microtubule growth in cultured neurons via the use of EB3-GFP (end-binding protein 3-green fluorescent protein). J Neurosci 2003;23:2655–2664.
41. Jordan MA, Thrower D, Wilson L. Effects of vinblastine, podophyllotoxin and nocodazole on mitotic spindles. Implications for the role of microtubule dynamics in mitosis. J Cell Sci 1992;102:401–416.
42. Perez F, Diamantopoulos GS, Stalder R, Kreis TE. CLIP-170 highlights growing microtubule ends in vivo. Cell 1999;96:517–527.
43. Hunt SD, Stephens DJ. The role of motor proteins in endosomal sorting. Biochem Soc Trans 2011;39:1179–1184.
44. Allan VJ. Cytoplasmic dynein. Biochem Soc Trans 2011;39:1169–1178.
45. Hirokawa N, Noda Y, Tanaka Y, Niwa S. Kinesin superfamily motor proteins and intracellular transport. Nat Rev Mol Cell Biol 2009;10:682–696.
46. Falcon-Perez JM, Nazarian R, Sabatti C, Dell'Angelica EC. Distribution and dynamics of Lamp1-containing endocytic organelles in fibroblasts deficient in BLOC-3. J Cell Sci 2005;118:5243–5255.
47. Toba S, Watanabe TM, Yamaguchi-Okimoto L, Toyoshima YY, Higuchi H. Overlapping hand-over-hand mechanism of single molecular motility of cytoplasmic dynein. Proc Natl Acad Sci U S A 2006;103:5741–5745.
48. Mallik R, Carter BC, Lex SA, King SJ, Gross SP. Cytoplasmic dynein functions as a gear in response to load. Nature 2004;427:649–652.
49. Kobayashi T, Murayama T. Cell cycle-dependent microtubule-based dynamic transport of cytoplasmic dynein in mammalian cells. PLoS One 2009;4:e7827.
50. Firestone AJ, Weinger JS, Maldonado M, Barlan K, Langston LD, O'Donnell M, Gelfand VI, Kapoor TM, Chen JK. Small-molecule inhibitors of the AAA+ ATPase motor cytoplasmic dynein. Nature 2012;484:125–129.
51. Schroer TA. Dynactin. Annu Rev Cell Dev Biol 2004;20:759–779.
52. Lencer WI, Constable C, Moe S, Rufo PA, Wolf A, Jobling MG, Ruston SP, Madara JL, Holmes RK, Hirst TR. Proteolytic activation of cholera toxin and Escherichia coli labile toxin by entry into host epithelial cells. Signal transduction by a protease-resistant toxin variant. J Biol Chem 1997;272:15562–15568.
53. Renard HF, Simunovic M, Lemiere J, Boucrot E, Garcia-Castillo MD, Arumugam S, Chambon V, Lamaze C, Wunder C, Kenworthy AK, Schmidt AA, McMahon HT, Sykes C, Bassereau P, Johannes L. Endophilin-A2 functions in membrane scission in clathrin-independent endocytosis. Nature 2015;517:493–496.
54. Galic M, Jeong S, Tsai FC, Joubert LM, Wu YI, Hahn KM, Cui Y, Meyer T. External push and internal pull forces recruit curvature-sensing N-BAR domain proteins to the plasma membrane. Nat Cell Biol 2012;14:874–881.
55. Meunier B, Quaranta M, Daviet L, Hatzoglou A, Leprince C. The membrane-tubulating potential of amphiphysin 2/BIN1 is dependent on the microtubule-binding cytoplasmic linker protein 170 (CLIP-170). Eur J Cell Biol 2009;88:91–102.
56. Wassmer T, Attar N, Harterink M, van Weering JR, Traer CJ, Oakley J, Goud B, Stephens DJ, Verkade P, Korswagen HC, Cullen PJ. The retromer coat complex coordinates endosomal sorting and dynein-mediated transport, with carrier recognition by the trans-Golgi network. Dev Cell 2009;17:110–122.
57. Traer CJ, Rutherford AC, Palmer KJ, Wassmer T, Oakley J, Attar N, Carlton JG, Kremerskothen J, Stephens DJ, Cullen PJ. SNX4

coordinates endosomal sorting of TfnR with dynein-mediated transport into the endocytic recycling compartment. Nat Cell Biol 2007;9:1370–1380.
58. Hong Z, Yang Y, Zhang C, Niu Y, Li K, Zhao X, Liu JJ. The retromer component SNX6 interacts with dynactin p150(Glued) and mediates endosome-to-TGN transport. Cell Res 2009;19:1334–1349.
59. Soppina V, Rai AK, Ramaiya AJ, Barak P, Mallik R. Tug-of-war between dissimilar teams of microtubule motors regulates transport and fission of endosomes. Proc Natl Acad Sci U S A 2009;106:19381–19386.
60. Verma P, Ostermeyer-Fay AG, Brown DA. Caveolin-1 induces formation of membrane tubules that sense actomyosin tension and are inhibited by polymerase I and transcript release factor/cavin-1. Mol Biol Cell 2010;21:2226–2240.
61. McNally FJ. Mechanisms of spindle positioning. J Cell Biol 2013;200:131–140.
62. Laan L, Pavin N, Husson J, Romet-Lemonne G, van Duijn M, Lopez MP, Vale RD, Julicher F, Reck-Peterson SL, Dogterom M. Cortical dynein controls microtubule dynamics to generate pulling forces that position microtubule asters. Cell 2012;148:502–514.
63. Redemann S, Pecreaux J, Goehring NW, Khairy K, Stelzer EH, Hyman AA, Howard J. Membrane invaginations reveal cortical sites that pull on mitotic spindles in one-cell C. elegans embryos. PLoS One 2010;5:e12301.
64. van Deurs B, von Bulow F, Vilhardt F, Holm PK, Sandvig K. Destabilization of plasma membrane structure by prevention of actin polymerization. Microtubule-dependent tubulation of the plasma membrane. J Cell Sci 1996;109:1655–1665.
65. Chinnapen DJ, Hsieh WT, te Welscher YM, Saslowsky DE, Kaoutzani L, Brandsma E, D'Auria L, Park H, Wagner JS, Drake KR, Kang M, Benjamin T, Ullman MD, Costello CE, Kenworthy AK, et al. Lipid sorting by ceramide structure from plasma membrane to ER for the cholera toxin receptor ganglioside GM1. Dev Cell 2012;23:573–586.
66. Hsieh WT, Hsu CJ, Capraro BR, Wu T, Chen CM, Yang S, Baumgart T. Curvature sorting of peripheral proteins on solid-supported wavy membranes. Langmuir 2012;28:12838–12843.
67. Lauvrak SU, Walchli S, Iversen TG, Slagsvold HH, Torgersen ML, Spilsberg B, Sandvig K. Shiga toxin regulates its entry in a Syk-dependent manner. Mol Biol Cell 2006;17:1096–1109.
68. Hehnly H, Sheff D, Stamnes M. Shiga toxin facilitates its retrograde transport by modifying microtubule dynamics. Mol Biol Cell 2006;17:4379–4389.
69. Tetaud C, Falguieres T, Carlier K, Lecluse Y, Garibal J, Coulaud D, Busson P, Steffensen R, Clausen H, Johannes L, Wiels J. Two distinct Gb3/CD77 signaling pathways leading to apoptosis are triggered by anti-Gb3/CD77 mAb and verotoxin-1. J Biol Chem 2003;278:45200–45208.
70. Steffensen R, Carlier K, Wiels J, Levery SB, Stroud M, Cedergren B, Nilsson Sojka B, Bennett EP, Jersild C, Clausen H. Cloning and expression of the histo-blood group Pk UDP-galactose: Ga1beta-4G1cbeta1-cer alpha1, 4-galactosyltransferase. Molecular genetic basis of the p phenotype. J Biol Chem 2000;275:16723–16729.
71. Choy E, Chiu VK, Silletti J, Feoktistov M, Morimoto T, Michaelson D, Ivanov IE, Philips MR. Endomembrane trafficking of Ras: the CAAX motif targets proteins to the ER and Golgi. Cell 1999;98:69–80.
72. Quintyne NJ, Gill SR, Eckley DM, Crego CL, Compton DA, Schroer TA. Dynactin is required for microtubule anchoring at centrosomes. J Cell Biol 1999;147:321–334.
73. Pralle A, Keller P, Florin EL, Simons K, Horber JK. Sphingolipid-cholesterol rafts diffuse as small entities in the plasma membrane of mammalian cells. J Cell Biol 2000;148:997–1008.
74. Kenworthy AK, Nichols BJ, Remmert CL, Hendrix GM, Kumar M, Zimmerberg J, Lippincott-Schwartz J. Dynamics of putative raft-associated proteins at the cell surface. J Cell Biol 2004;165:735–746.
75. Zacharias DA, Violin JD, Newton AC, Tsien RY. Partitioning of lipid-modified monomeric GFPs into membrane microdomains of live cells. Science 2002;296:913–916.
76. Schindelin J, Arganda-Carreras I, Frise E, Kaynig V, Longair M, Pietzsch T, Preibisch S, Rueden C, Saalfeld S, Schmid B, Tinevez JY, White DJ, Hartenstein V, Eliceiri K, Tomancak P, et al. Fiji: an open-source platform for biological-image analysis. Nat Methods 2012;9:676–682.
77. Nehls S, Snapp EL, Cole NB, Zaal KJ, Kenworthy AK, Roberts TH, Ellenberg J, Presley JF, Siggia E, Lippincott-Schwartz J. Dynamics and retention of misfolded proteins in native ER membranes. Nat Cell Biol 2000;2:288–295.
78. Day CA, Kenworthy AK. Mechanisms underlying the confined diffusion of cholera toxin B-subunit in intact cell membranes. PLoS One 2012;7:e34923.
79. Umemura K, Kimura H. Hydrogen sulfide enhances reducing activity in neurons: neurotrophic role of H2S in the brain? Antioxid Redox Signal 2007;9:2035–2041.
80. Macia E, Ehrlich M, Massol R, Boucrot E, Brunner C, Kirchhausen T. Dynasore, a cell-permeable inhibitor of dynamin. Dev Cell 2006;10:839–850.
81. Cole NB, Sciaky N, Marotta A, Song J, Lippincott-Schwartz J. Golgi dispersal during microtubule disruption: regeneration of Golgi stacks at peripheral endoplasmic reticulum exit sites. Mol Biol Cell 1996;7:631–650.
82. Goodwin JS, Drake KR, Rogers C, Wright L, Lippincott-Schwartz J, Philips MR, Kenworthy AK. Depalmitoylated Ras traffics to and from the Golgi complex via a nonvesicular pathway. J Cell Biol 2005;170:261–272.
83. Saslowsky DE, Cho JA, Chinnapen H, Massol RH, Chinnapen DJ, Wagner JS, De Luca HE, Kam W, Paw BH, Lencer WI. Intoxication of zebrafish and mammalian cells by cholera toxin depends on the flotillin/reggie proteins but not Derlin-1 or –2. J Clin Invest 2010;120:4399–4409.
84. Jaqaman K, Loerke D, Mettlen M, Kuwata H, Grinstein S, Schmid SL, Danuser G. Robust single-particle tracking in live-cell time-lapse sequences. Nat Methods 2008;5:695–702.